Nat Hazards
https://doi.org/10.1007/s11069-018-3257-4

ORIGINAL PAPER

Evaluation of tsunami inundation using synthetic aperture radar (SAR) data and numerical modeling

M. Iyyappan[1,2] · Tune Usha[1] · S. S. Ramakrishnan[2] · K. Srinivasa Raju[2] · G. Gopinath[1,2] · S. Chenthamil Selvan[1] · S. K. Dash[1] · P. Mishra[1]

Received: 14 March 2017 / Accepted: 4 March 2018

Abstract Little Andaman, the fourth largest island in the Andaman group of islands of India, was severely affected by the December 26, 2004, Indian Ocean tsunami generated by massive earthquake of moment magnitude 9.3 Mw which devastated the Andaman and Nicobar group of islands causing heavy damage to life and property. Due to hostile terrain conditions not much information was available on the extent of inundation and run-up along the island except for Hut Bay region. In order to study the vulnerability of the island to tsunami hazard, the inundation in the island due to the 2004 tsunami was studied using TUNAMI N2 numerical model and ENVISAT ASAR datasets. The extent of inundation derived from the SAR imagery was compared using the RTK-GPS field survey points collected in the Hut Bay regions immediately after the 2004 tsunami. The extent of inundation obtained from SAR images for the entire island was compared with inundation obtained from model. It was observed that the inundation obtained from the model matched well with inundation extent from SAR imagery for nearshore regions, while for low-lying areas and creeks large deviations were observed. In the absence of field datasets, the inundation derived from SAR imagery would be effective in providing ground data to validate the numerical models which can then be run for multiple scenarios for disaster mitigation and planning operation in areas that have hostile terrain conditions.

Keywords Little Andaman · India · SAR · Tsunami · TUNAMI N2

✉ M. Iyyappan
muthuiyyappan@gmail.com

[1] Integrated Coastal and Marine Area Management (ICMAM) -Project Directorate, Ministry of Earth Sciences, Government of India, Chennai 600100, India

[2] Institute of Remote Sensing (IRS), Anna University, Chennai 600025, India

Published online: 12 March 2018

1 Introduction

The second largest earthquake of magnitude Mw 9.3 in the last 200 years (Malik et al. 2006) and fifth largest since 1900 (Subramanian 2005) occurred on December 26, 2004, at the interface of the Indo-Burma Plates. It is a tectonic plate with high probability for megathrust earthquakes causing tsunami waves (Rajendran et al. 2003). In last 300 years, tsunamis are recorded 13 times in the Indian Ocean region and 3 of them are recorded in Andaman and Nicobar Islands (ICMAM-PD report 2005). Tsunami reached Andaman and Nicobar Islands between 40 and 50 min after the occurrence of earthquake (EERI Report 2005), which caused extensive damages in parts of the islands (Usha et al. 2009). The Andaman and Nicobar Islands are situated in active fault zone. The study area is categorized under Seismic Zone V with a high degree of risk (Ramanamurthy et al. 2005) and has experienced several earthquakes of moderate to large magnitude during the historic and recent past (Malik et al. 2006). It provides an ideal tectonic setting for the event of megathrust earthquakes and particularly for the effects of the tsunami waves generated by such events (Rajendran et al. 2003). The region is at risk not only from tsunamis generated by earthquakes from nearby sources along the Andaman arc, but also from adjacent regions such as Indonesia, as in the 2004 Great Sumatra earthquake (Malik et al. 2006). Information on the maximum extent of inundation and run-up is essential to plan for tsunami mitigation operations. Field measurement, remote sensing data and numerical models play a significant role in understanding areas prone to coastal inundation.

Field observations using GPS (Banerjee et al. 2005; Vigny et al. 2005; Chlieh et al. 2007) provide information such as deformation, geomorphological changes and tsunami inundation due to an earthquake. In situ measurements are sparse and difficult to measure (Is et al. 2007) and field surveys takes a lot of time (Suppasri et al. 2012) and may not cover entire area due to damaged roads and bridges, with much debris as obstacles (Suppasri et al. 2012), while remote sensing provides the information in space and time (Is et al. 2007; Kumar et al. 2008). Unlike optical sensors, radar images are widely used for disaster monitoring because of the capability of penetrating clouds and operating at adverse weather condition (Huang et al. 2015). Synthetic aperture radar (SAR) is significant for its ability to record the backscattering values of the Earth's surface (Henderson and Lewis 1998) which is dependent on the roughness of the ground surface and the dielectric constant. Based on this idea, the damaged and inundated areas due to tsunami are identified using the backscattering coefficient from pre- and post-event SAR images (Suppasri et al. 2012). SAR images can also be used to detect shoreline changes, inundation extent, seismic uplift and subsidence and vertical displacement (Tobita et al. 2006; Is et al. 2007), ground displacement associated with the earthquake (Kobayashi 2014) and tsunami damage investigation of built-up areas (Chen and Sato 2013).

The potential run-ups and inundation due to tsunami are determined by numerical modeling, which also provides information on wave travel time, wave heights and current velocities, which are important hazard parameters for damage analyses (Romer et al. 2012). To reproduce the correct wave dynamics during the inundation computations, high-resolution bathymetric and topographic grids are required (Usha et al. 2012).

2 Study area

Little Andaman is approximately 722 km^2 (92.37 to 92.59°E, 10.51 to 10.89°N) and is the furthest inhabited island among the Andaman Islands, located 120 km south of Port Blair. The island houses pristine beaches, sprawling palm oil plantations and waterfalls, and the population is primarily made up of people from Bengal and Tamil Nadu. The main settlement, Indira Bazaar, is 2 km north of the jetty at Hut Bay, and Little Andaman has a cult reputation among surfers for having some of the best conditions in South Asia. Though the 2004 tsunami caused large-scale damage to the island, Little Andaman has recovered fast due to recovery operations by Government of India. Figure 1 describes the study area index map.

3 Materials and methods

The rationale behind this study is that in the absence of proper field datasets, SAR datasets could provide the necessary information to validate the numerical models, which could then be used to capture multiple inundation scenarios to study the vulnerability of the island to tsunami hazard. The methodology flowchart for the calculation of the backscattering coefficient (dB) and tsunami inundation mapping is shown in Fig. 2.

Satellite remote sensing data provide fundamental information to evaluate areas involved in natural disasters because of their synoptic view capability. This approach was

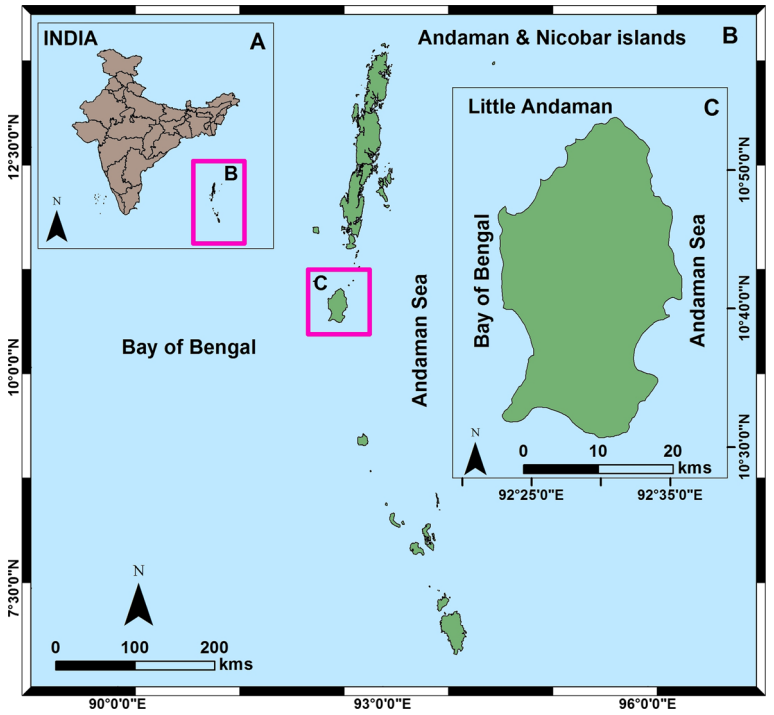

Fig. 1 Study area map

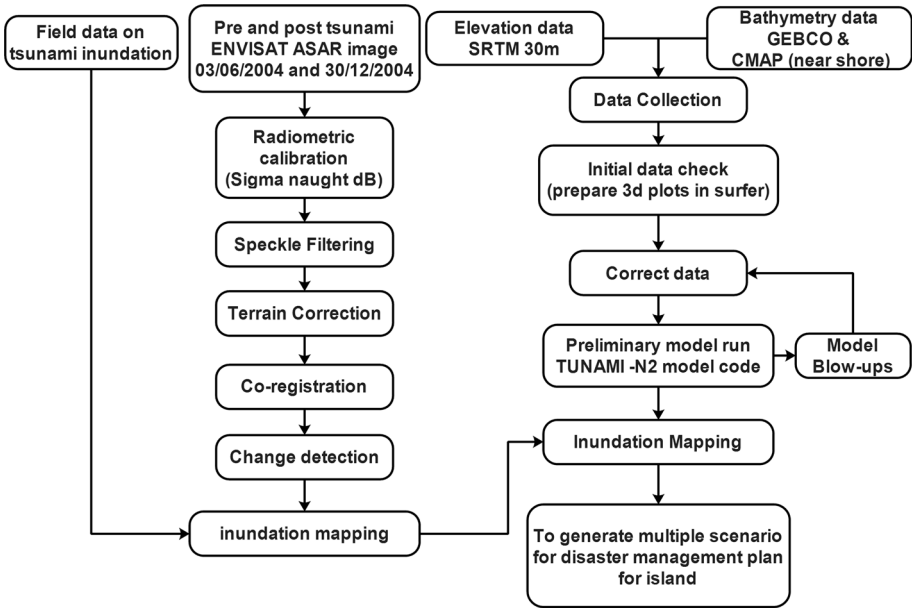

Fig. 2 Methodology flowchart adopted for this study

particularly effective for this tsunami event, which affected a very large area, making the extensive field survey unfeasible (Zhang et al. 2014). Among various sensors, SAR is remarkable for its ability to record the physical value of the Earth's surface (Henderson and Lewis 1998). Unlike optical sensors, SAR enables the observation of surface conditions day or night, even through clouds. SAR interferometric analyses using phase information have successfully provided quantification of relative ground displacement levels due to natural disasters (Massonnet et al. 1993). More importantly, intensity information obtained from SAR represents a physical value (backscattering coefficient) that is strongly dependent on the roughness of the ground surface and the dielectric constant (Suppasri et al. 2012). The SAR image provides stable image intensity, which is suitable for precise comparison and change detection. The moderate resolution of active sensors can quantify the vertical and horizontal movements of the Earth's surface due to earthquake and inundation limit of tsunami (Gillespie et al. 2007). Optical images obtained during the disaster time provides limited information due to cloud cover, and hence, it is difficult to interpret the extent of inundation. The environment satellite (ENVISAT) was launched by European Space Agency (ESA) in 2002. It carries an advanced synthetic aperture radar (ASAR) instrument that operates at C-band with a center frequency of 5.3 GHz, an incidence angle of 23°, a swath width of 100 km and a spatial resolution of 12.5 m. For this study, ENVISAT ASAR data were acquired on June 3, 2004 (VV-vertical transmit and vertical receive), and December 30, 2004, (HH-horizontal transmit and horizontal receive) polarizations. The characteristics of ENVISAT ASAR satellite images are shown in Table 1.

Table 1 Characteristics of ENVISAT ASAR satellite images

Track	Frame	Orbit	Swath	Mode	Polarization	Acquisition data
233	3375	11810	IS2	Descending	VV	June 3, 2004
233	3375	14816	IS2	Descending	HH	December 30, 2004

3.1 Calculation of backscattering coefficient (dB) and tsunami inundation mapping from ENVISAT ASAR data

SAR data for Andaman and Nicobar Islands were obtained from European Space Agency (ESA). ENVISAT ASAR image mode precision (IMP) image of level 1b products were preprocessed using sentinel application platform (SNAP) for Little Andaman. Pre- and post-tsunami SAR data were imported into SNAP toolbox radiometrically calibrated, and the backscattering coefficient (sigma naught, dB) was calculated. For speckle filtering, various filters were evaluated and it was found that Lee and Frost gave the best filtering result for ASAR images (Wang et al. 2012). The geometrically corrected pre- and post-tsunami backscattering (dB) images of ENVISAT ASAR data for Little Andaman are shown in Fig. 3. The backscattering images were co-registered, and a change analysis was performed using pre- and post-tsunami backscatter images to identify the extent of inundation along the coastal areas.

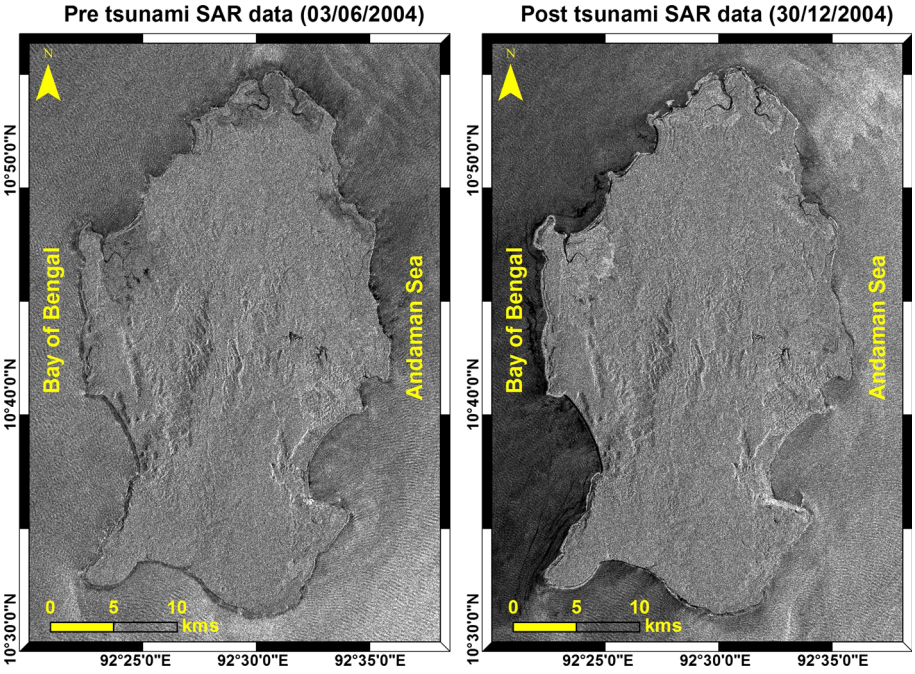

Fig. 3 Backscattering (dB) images of pre- and post-tsunami

3.2 Tsunami inundation from TUNAMI N2 model

Numerical models have been used in recent years for tsunami generation, propagation and interaction with the coastal areas (Usha et al. 2009). TUNAMI N2 model was used for modeling which is based on linear theory in deep waters, shallow-water theory in shallow waters, and run-up on land with constant grids (Nayak et al. 2012). The TUNAMI N2 code was originally developed by Prof. Fumihiko Imamura in Disaster Control Research Centre in Tohoku University (Japan). The TUNAMI N2 modeling process can be divided into three stages: generation, propagation and inundation (Synolakis 2004). Generation forms the first stage in the modeling of tsunami and includes the calculation of initial disturbance of the ocean surface due to the earthquake-triggered deformation of the sea floor. Most studies of tectonic tsunamis use Mansinha and Smylie's (1971) analytical formula to predict the seafloor displacement due to an earthquake and to model initial water displacement (Legg et al. 2004). Many studies were carried out using TUNAMI N2 model along the Indian Coast to study the impact of 2004 Sumatra tsunami (Ramanamurthy et al. 2005; Usha et al. 2012; Nayak et al. 2012; Praveen et al. 2013; Mishra et al. 2014; Selvan and Kankara 2016).

3.3 Bathymetry and topography

To reproduce the correct wave dynamics during inundation, accurate and high-resolution bathymetry and topography data are essential. The information of "nearshore" topography and bathymetry plays an important role in predicting the tsunami wave propagation, run-up height and inundation extent accurately. The SRTM (30 and 90 m) and ASTER (30 m) DEMs are only available for Little Andaman Island. Praveen et al. (2013) used SRTM 90 m DEM to run the TUNAMI N2 model run for coastal areas of Kerala, India. The available high-resolution topography data for Little Andaman were extracted from SRTM 30 m DEM. The coastal bathymetric data, that is, from 150 m depth to coast, were extracted from C-Map for "nearshore" areas, and deep-sea bathymetry was extracted from general bathymetric chart of the oceans (GEBCO) data from tsunami-originating source to 150 m depth along the coast (Usha et al. 2012; Gopinath et al. 2014; Mishra et al. 2014; Selvan and Kankara 2016). The bathymetry and topography details are given in Table 2.

The grid spacing for A, B, C and D was decided based on Courant–Friedrichs–Lewy (CFL) criteria (numerical stability). The grid spacing implemented in the model for A, B, C and D is 81′ (2430 m), 27′ (810 m), 9′ (270 m) and 3′ (90 m), respectively. Grids A, B and C were set as linear mode, while grid D was set in a nonlinear mode. The nonlinear model considers the flooding/drying of land portion and amplification of the wave due to bathymetry. The bathymetry and topography data were merged and exported as a XYZ text file format. The XYZ data were imported to Surfer software and interpolated using kriging interpolation technique into four nested regular bathymetry grids for A (81′) to D (3′) to be used in TUNAMI N2 model. Then, seismic parameters were adopted from Usha et al. (2012); Mishra et al. (2014); and Selvan and Kankara (2016), using that the five different

Table 2 Details of bathymetry and topography data used in the model

S. No.	Bathymetry/topography	Resolution
1	GEBCO	30 arcsec ($\sim$ 990 m)
2	C-Map	3 arcsec (90 m)
3	SRTM	1 arcsec (30 m)

fault zones were generated and then combined together for the generation of initial sea surface elevation of the 2004 Sumatra tsunami. In this study the algorithm of Mansinha and Smylie (1971) was used to calculate the seafloor deformation. The initial sea surface deformation at fault zone is shown Fig. 4. The input seismic parameters used in the study are shown in Table 3. Tsunami waves travel outward in all directions from the originating area, with the direction of the main energy propagation generally being orthogonal to the direction of the earthquake rupture zone. The tsunami wave propagating from the deep sea undergoes a change, and the wave height is increased at the coast due to the "nearshore" bathymetry and coastal morphology. The run-up and inundation limit of the tsunami on land is the final output of the tsunami model. Inundation results were carried out at 90 m grid resolution, and hence, the results were studied considering the acceptable modeling error of 90 m ($\sim$ 1 grid). The inundation limit obtained from numerical model was then compared with the inundation of SAR image.

3.4 Ground truth verification

After tsunami event, field data on the extent of inundation and run-up were collected using RTK-GPS in various coastal stretches of Indian coast including Andaman and Nicobar Islands (Ramanamurthy et al. 2005). Field verification was conducted only for accessible areas.

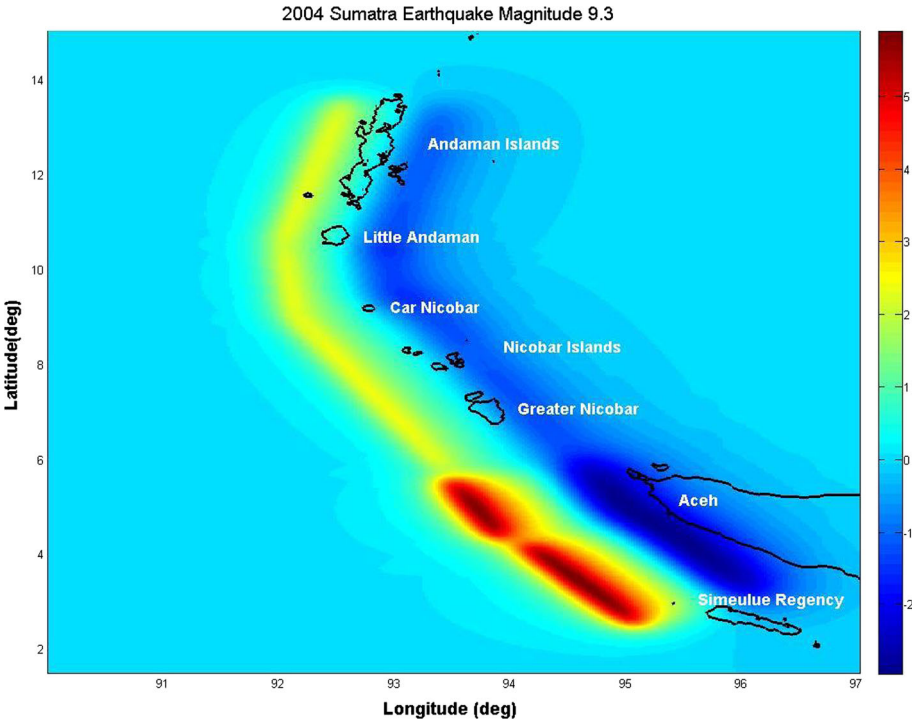

Fig. 4 Initial sea surface elevation computed for 2004 Sumatra using Mansinha and Smylie theory

Table 3 Details of seismic parameters used in the model

Parameters	Sumatra (2004)				
	Block 1	Block 2	Block 3	Block 4	Block 5
Lat (°)	95.10	93.90	93.41	92.10	92.00
Long (°)	2.50	4.33	5.80	9.10	10.50
Fault length (km)	220	150	390	150	350
Fault width (km)	130	130	120	95	95
Strike (°)	323	348	338	356	10
Slip (m)	18	23	12	12	12
Dip (°)	12	12	12	12	12
Rake (°)	90	90	90	90	90
Depth (km)	25	25	25	25	25

4 Results and discussion

4.1 Inundation mapping from SAR images

The extent of inundation along Little Andaman due to 2004 tsunami was mapped by analyzing the changes in the backscattering values of the pre- and post-SAR images. In the post-tsunami image the backscattering values were high due to high soil moisture and the debris left behind by the receding tsunami waves. Backscattering values increase since the surface roughness increases due to the debris and there is also an increase in the dielectric constant due to increased soil moisture. Thus, the surface scattering was enhanced, while the double-bounce scattering was reduced consequently (Chen and Sato 2013). The inundation extent obtained from the SAR images was validated using the field measurements, which was collected after tsunami using RTK-GPS for Hut Bay of Little Andaman (Ramanamurthy et al. 2005). The inundation had occurred to a maximum distance of 1200 m in Hut Bay from the shore (Ramanamurthy et al. 2005). The maximum extent of inundation at Hut Bay from SAR image analysis was approximately 1260 m (Fig. 5). The resolution of SAR image is 12.5 m used for this study and inundation limit extracted visually in GIS environment and comparison with RTK-GPS field data may be varied approximately $\pm$ 2 pixels. The European Space Agency (ESA) reported that the accuracy of ENVISAT ASAR data is 30 m. Table 4 shows the difference between observed inundation from field and estimated inundation from SAR images.

It is evident that the inundation obtained from SAR images matched well with the field data. Since there were no field measurements for the other parts of the island except Hut Bay, the inundation for the entire island was studied and it was found that the maximum inundation occurred in Jackson creek, Bumila creek and Dugong creek in the western, northern and northeastern side of Little Andaman, respectively (Fig. 6). These creeks have mangrove swamps, and normally, HH polarization image gives low backscattering values for vegetation when compared to VV polarization image. However, in the post-tsunami images inundated vegetation appears to have high backscattering values in the HH polarization image.

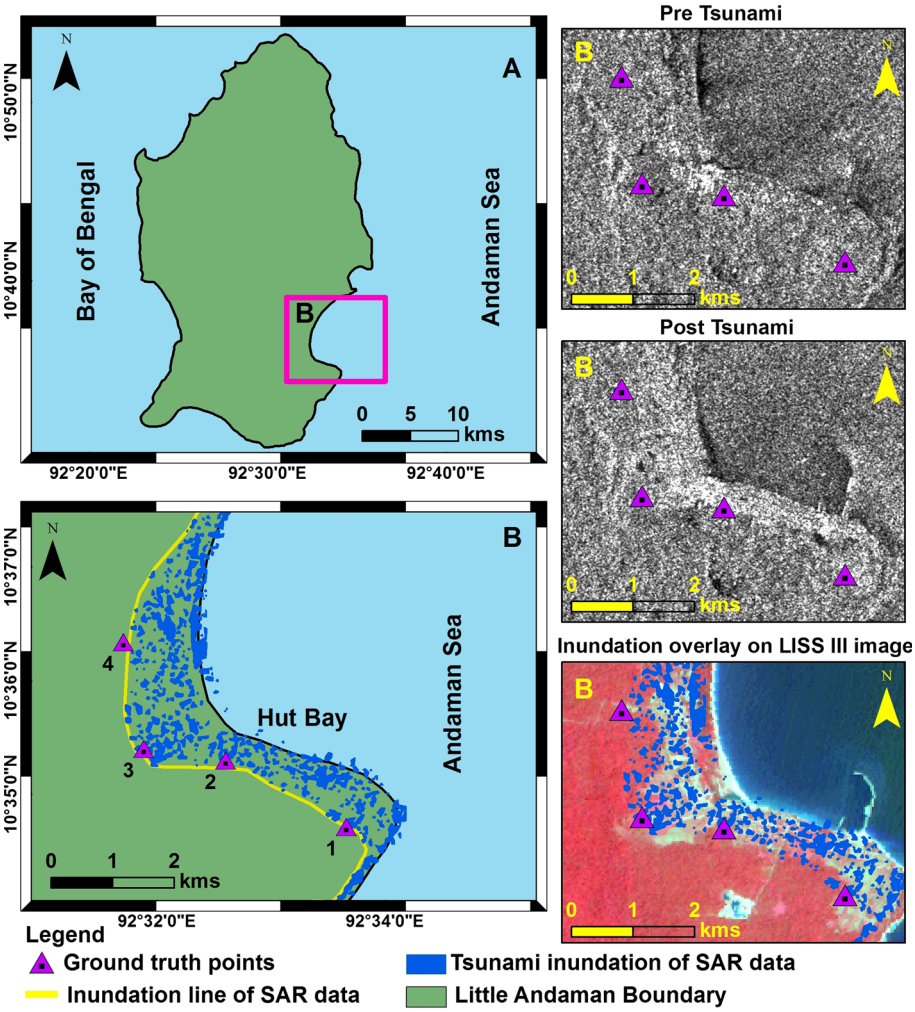

Fig. 5 Tsunami inundation extent from SAR images at Hut Bay of Little Andaman

Table 4 Observed inundation from field and that estimated from SAR images

Point no.	Location	Longitude (dd)	Latitude (dd)	Observed (m)	Estimated (m)
1	Near Indira Bazaar	92.560	10.578	645	605
2	Settlement/agriculture/forest	92.543	10.588	401	520
3	Near PWD guest house	92.531	10.590	1200	1260
4	Settlement/agriculture/forest	92.528	10.605	1050	950

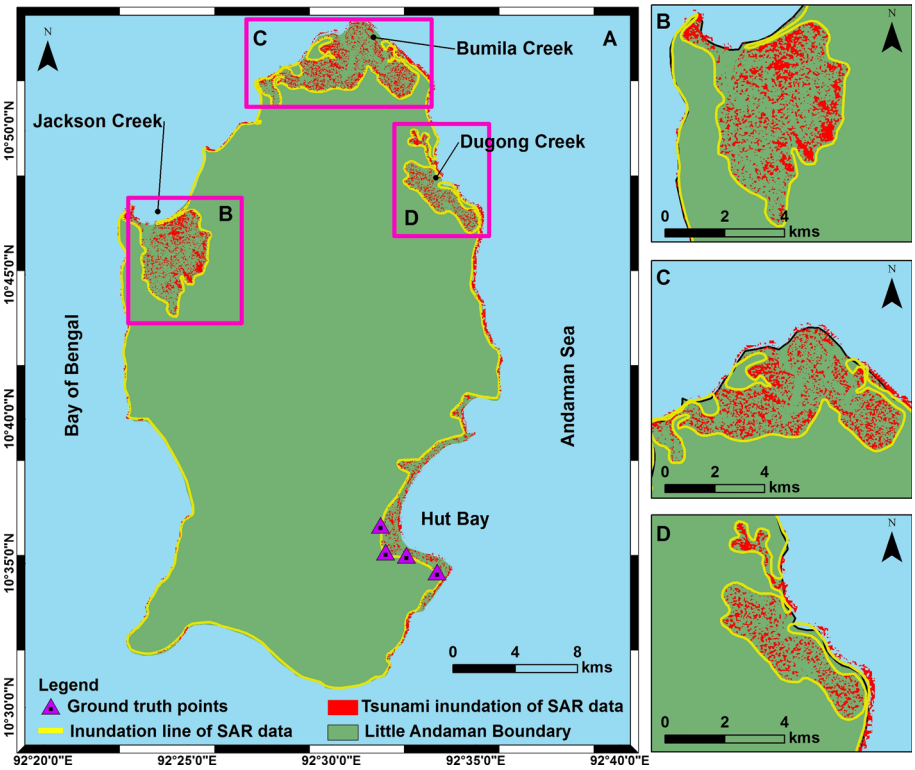

Fig. 6 Maximum tsunami inundation extents from SAR images at various locations in Little Andaman

4.2 Tsunami inundation modeling results (TUNAMI N2 model)

The maximum inundation distance obtained due to 2004 Sumatra was 1450 m at locations 2. Inundation at this particular location is due to the Bumila creek where the wave travels to long distance. Location 4 shows a tsunami run-up to a distance of 1347 m in Jackson creek. Locations 3 (98 m), 5 (107 m) and 10 (94 m) show least inundation distance in nearshore areas. The inundation distance obtained all along the study area is shown in Fig. 7.

The inundation from TUNAMI N2 model was compared with the inundation extent obtained from SAR images as shown in Table 5 and Fig. 7. From the SAR data it was observed that the Eastern side of the island was inundated more when compared to the western side and this could probably be attributed to the emergence observed in Andaman and Nicobar group of islands due to 2004 Sumatra earthquake (Tobita et al. 2006; Chini et al. 2008). It was also observed that though the inundations matched well in the nearshore areas, there were discrepancies in mapping the inundation along and through the creeks and in the western side of the islands. The TUNAMI N2 model using SRTM 30 m DEM underestimated the inundation limits for creeks and low-lying areas. The large vertical errors and poor resolution of the coastline in the SRTM elevation datasets cause the modeled inundation limits, and it should not be used to underpin tsunami inundation model (Griffin et al. 2015). The recommendation of using DTM derived from interferometric SAR (InSAR) for modeling tsunami inundation limits (Griffin et al. 2015) will be carried

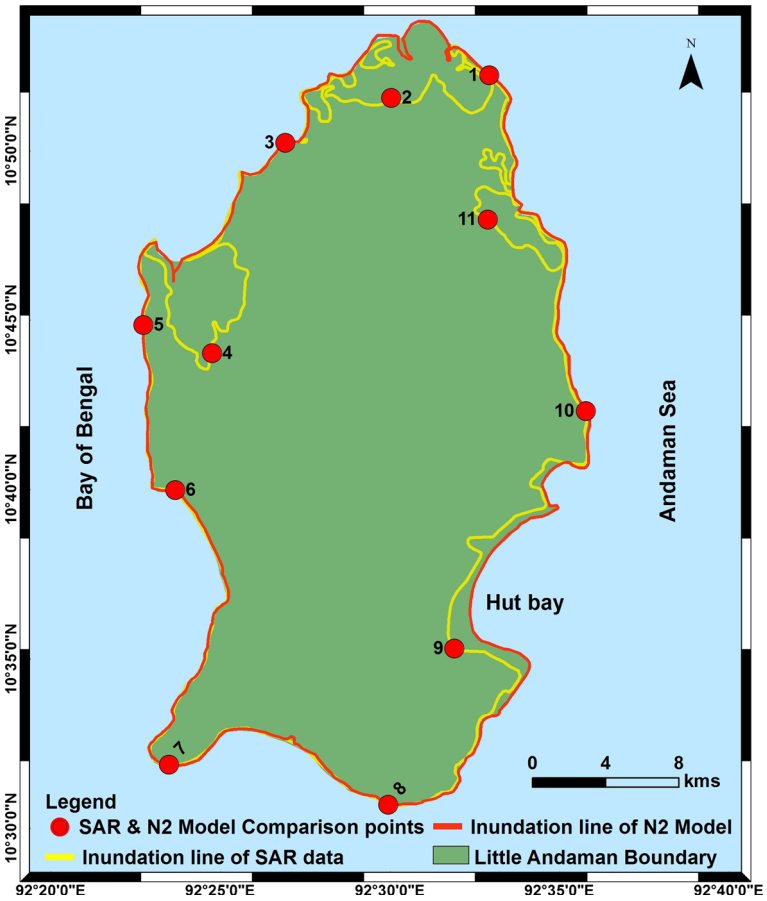

Fig. 7 Comparison between estimated inundation from SAR imagery and TUNAMI N2 model

out for future. Data acquisition for InSAR requires same look angle, pass direction (ascending/descending), incidence angle, relative orbit, imaging mode, wavelength and small baseline between satellites (Tobita et al. 2006).

5 Conclusion

The inundation limit was mapped for Little Andaman due to 2004 tsunami using pre- and post-SAR images. The inundation limits obtained from the SAR images were compared with RTK-GPS field measurements. The inundation limits nearly matched the field measurements. The inundation limit values obtained from TUNAMI N2 model were compared with inundation limit from SAR images. The inundation limits nearly matched in the nearshore areas only, and there were discrepancies in mapping the inundation along and through the creeks and in the western side of the islands. The SRTM 30 m DEM underestimated the inundation limits for creeks and low-lying areas. SAR image interpretation is complicated because SAR records backscatter signal, subject to considerable noise, and

Table 5 Comparison of inundation between SAR and TUNAMI N2 at different locations

Point No.	Longitude	Latitude	Inundation from SAR images (m)	Model-predicted inundation (m)
1	92.55	10.87	216	152
2*	92.50	10.86	3314	1450
3	92.45	10.84	110	98
4*	92.41	10.73	4251	1347
5	92.38	10.75	113	107
6	92.39	10.67	215	209
7	92.39	10.53	173	153
8	92.50	10.51	246	203
9	92.53	10.59	1200	172
10	92.60	10.71	164	94
11*	92.55	10.80	1834	323

*Points 2, 4 and 11 pertain to creeks

side-looking sensor causes shadow, foreshortening and layover that can occur in SAR image based on the topography. The revisit time between the before- and after-disaster image pair should be minimal to avoid the influences of temporal changes which were not caused by the natural disaster (e.g., clearing of the debris after the event, or construction activities, etc.). Disaster management benefits strongly from high-resolution SAR for precise measurement of distances, which can be used for the creation of precise height models using InSAR. The TUNAMI N2 model's limitations are as follows: The finest model grid size was 90 m due to the limitation of data and computational resources, model flow up when high peak appear in the bathymetry and source uncertainty. This study is essentially to show how numerical models and SAR datasets can be used to study the vulnerability of coastal areas to ocean-originating hazards, especially for island regions wherein no actual field data are available to compare the output of the numerical models. In order to develop a disaster management plan for relative inaccessible areas such as islands there is a need to develop a database on various possible inundation scenarios by varying the possible source parameters. The inundation limits of SAR and TUNAMI N2 model can be used to generate the hindcast or forecast of the inundation for various tsunamigenic sources (Sumatra 2004, North Andaman 1941, Car Nicobar 1881, Arakan 1762 and Makran 1945 for Indian region).

Acknowledgements We are grateful to European Space Agency (ESA) for providing ENVISAT ASAR and ERS SAR datasets for Andaman and Nicobar Islands at free of cost. Authors would like to thank Integrated Coastal and Marine Area Management Project Directorate (ICMAM-PD), Ministry of Earth Sciences, Government of India, for providing RTK- GPS field data, collected immediately after the tsunami, for this research work.

References

Banerjee P, Pollitz FF, Burgmann R (2005) The size and duration of the Sumatra–Andaman earthquake from far-field static offsets. Science 308:1769–1772. https://doi.org/10.1126/science.1113746

Chen SW, Sato M (2013) Tsunami damage investigation of built-up areas using multitemporal spaceborne full polarimetric SAR images. IEEE Trans Geosci Remote Sens 51(4):1985–1997. https://doi.org/10.1109/TGRS.2012.2210050

Chini M, Bignami C, Stramondo S, Pierdicca N (2008) Uplift and subsidence due to the 26 December 2004 Indonesian earthquake detected by SAR data. Int J Remote Sens 29(13):3891–3910. https://doi.org/10.1080/01431160701871112

Chlieh M, Avouac JP, Hjorleifsdottir V et al (2007) Coseismic slip and afterslip of the great Mw 9.15 Sumatra–Andaman earthquake of 2004. Bull Seismol Soc Am 97(1A):152–173. https://doi.org/10.1785/0120050631

EERI Special Earthquake Report (2005) The Great Sumatra Earthquake and Indian Ocean Tsunami of December 26, 2004

Gillespie TW, Chu J, Frankenberg E, Thomas D (2007) Assessment and prediction of natural hazards from satellite imagery. Prog Phys Geogr 31(5):459–470. https://doi.org/10.1177/0309133307083296

Gopinath G, Løvholt F, Kaiser G et al (2014) Impact of the 2004 Indian Ocean tsunami along the Tamil Nadu coastline: field survey review and numerical simulations. Nat Hazards 72(2):743–769. https://doi.org/10.1007/s11069-014-1034-6

Griffin J, Latief H, Kongko W et al (2015) An evaluation of onshore digital elevation models for modeling tsunami inundation zones. Front Earth Sci 3(32):1–16. https://doi.org/10.3389/feart.2015.00032

Henderson FM, Lewis AJ (1998) Principles and applications of imaging radar, manual of remote sensing, 3rd edition, volume 2. Eos 80(6):67

Huang SQ, You H, Wang YT (2015) Environmental monitoring of natural disasters using synthetic aperture radar image multi-directional characteristics. Int J Remote Sens 36(12):3160–3183. https://doi.org/10.1080/01431161.2015.1041171

ICMAM-PD report (2005) Preliminary assessment of impact of tsunami in selected coastal areas of India. 2005:1–42

Is P, Foumelis M, Lekkas E (2007) Vertical tectonic motion in Andaman Islands detected by multi-temporal satellite radar images. Bull Geol Soc Greece XXXX:1–12

Kobayashi T (2014) Remarkable ground uplift and reverse fault ruptures for the 2013 Bohol earthquake (Mw 7.1), Philippines, revealed by SAR pixel offset analysis. Geosci Lett 1(7):1–10. https://doi.org/10.1186/2196-4092-1-7

Kumar CS, Murugan PA, Krishnamurthy RR et al (2008) Inundation mapping—a study based on December 2004 Tsunami Hazard along Chennai coast, Southeast India. Nat Hazards Earth Syst Sci 8(4):617–626. https://doi.org/10.5194/nhess-8-617-2008

Legg MR, Borrero JC, Synolakis CE (2004) Tsunami hazards associated with the Catalina Fault in southern California. Earthq Spectra 20(3):917–950. https://doi.org/10.1193/1.1773592

Malik JN, Murty CVR, Rai DC (2006) Landscape changes in the Andaman and Nicobar Islands (India) after the December 2004 great Sumatra earthquake and Indian Ocean tsunami. Earthq Spectra 22(S3):43–66. https://doi.org/10.1193/1.2206792

Mansinha L, Smylie DE (1971) The displacement fields of inclined faults. Bull Seismol Soc Am 61:1400–1433

Massonnet D, Rossi M, Carmona C et al (1993) The displacement field of the Landers earthquake mapped by radar interferometry. Nature 364:138–142

Mishra P, Usha T, Ramanamurthy MV (2014) Evaluation of tsunami vulnerability along northeast coast of India. Cont Shelf Res 79:16–22. https://doi.org/10.1016/j.csr.2014.02.007

Nayak S, Usha T, Kankara RS, Reddy NT (2012) Tsunami inundation modeling and mapping using ALTM- and CARTOSAT-derived coastal topographic data. Mar Geod 35:429–440. https://doi.org/10.1080/01490419.2011.646606

Praveen SS, Kurian NP, Hameed TSS (2013) Tsunami inundation modelling for the Coast of Kerala, India. Mar Geod 36(1):86–97. https://doi.org/10.1080/01490419.2012.699502

Rajendran CP, Earnest A, Rajendran K et al (2003) The 13 September 2002 North Andaman (Diglipur) earthquake: an analysis in the context of regional seismicity. Curr Sci 84(7):919–924

Ramanamurthy MV, Sundaramoorthy S, Pari Y et al (2005) Inundation of sea water in Andaman and Nicobar Islands and parts of Tamil Nadu coast during 2004 Sumatra tsunami. Curr Sci 88(11):1736–1740

Romer H, Willroth P, Kaiser G et al (2012) Potential of remote sensing techniques for tsunami hazard and vulnerability analysis-a case study from Phang-Nga province, Thailand. Nat Hazards Earth Syst Sci 12:2103–2126. https://doi.org/10.5194/nhess-12-2103-2012

Selvan SC, Kankara RS (2016) Tsunami model simulation for 26 December 2004 and its effect on Koodankulam region of Tamil Nadu Coast. Int J Ocean Clim Syst 7(2):62–69. https://doi.org/10.1177/1759313115623165

Subramanian BR (2005) Impact of 26th December 2004 Tsunami in Andaman and Nicobar Islands and establishment of warning system. Wave in Bay ENVIS Publication Series 3/2005

Suppasri A, Koshimura S, Matsuoka M et al (2012) Application of remote sensing for tsunami disaster. Remote Sens Planet Earth. https://doi.org/10.5772/32136

Synolakis CE (2004) Tsunami and Seiche. In: Chen WF, Scawthorn C (eds) Earthquake engineering handbook. CRC Press, Washington

Tobita M, Suito H, Imakiire T et al (2006) Outline of vertical displacement of the 2004 and 2005 Sumatra earthquakes revealed by satellite radar imagery. Earth Planets Space 58:1–4. https://doi.org/10.1186/BF03351906

Usha T, Ramanamurthy MV, Reddy NT, Murty TS (2009) Vulnerability assessment of Car Nicobar to tsunami hazard using numerical model. Sci Tsunami Hazards 28(1):15–34

Usha T, Ramanamurthy MV, Reddy NT, Mishra P (2012) Tsunami vulnerability assessment in urban areas using numerical model and GIS. Nat Hazards 60:135–147. https://doi.org/10.1007/s11069-011-9957-7

Vigny C, Simons WJF, Abu S et al (2005) Insight into the 2004 Sumatra–Andaman earthquake from GPS measurements in southeast Asia. Nature 436:201–206. https://doi.org/10.1038/nature03937

Wang X, Ge L, Xiaojing L (2012) Evaluation of filters for ENVISAT ASAR speckle suppression in pasture area. XXII ISPRS Congr 1–7:341–346. https://doi.org/10.5194/isprsannals-I-7-341-2012

Zhang Y, Jiang Z, Fang Y, Cheng X (2014) Analysis and interpretation of tsunami damage caused by the 2011 Japan earthquake using ENVISAT ASAR images. IOP Conf Ser Earth Environ Sci 17:1–6. https://doi.org/10.1088/1755-1315/17/1/012089